DOI: 10.26599/FSHW.2025.9250725

Contents lists available at SciOpen

Food Science and Human Wellness

journal homepage: https://www.sciopen.com/journal/2097-0765

China Food Publishing Co.

Crosstalk mechanism exploration of the medical food homology compound β-ecdysterone with sympathetic overactivation-induced cardiac hypertrophy

Yu Duan[1†], Xin Li[2†], Runze Li[3,4†], Ming Jiang[5], Qinhao Zhou[3,4], Yu Jiao[7], Siqi Peng[8], Yan Lin[9*], Hui Li[10*], Dan Xiao[4,5*]

[1]*Department of Cardiology, The Fourth Affiliated Hospital of Harbin Medical University， Harbin, Heilongjiang 150001, China*

[2]*Department of Psychiatry, The Fourth Affiliated Hospital of Qiqihar Medical University, Qiqihar, Heilongjiang, China*

[3]*National and Local Joint Engineering Laboratory for Synthesis Transformation and Separation of Extreme Environmental Nutrients, Harbin Institute of Technology, Harbin, Heilongjiang 150001, China,*

[4]*Zhengzhou Research Institute, Harbin Institute of Technology, Zhengzhou, Henan, 450007, China*

[5]*Department of Public Health, Qiqihar Medical University ， Qiqihar, Heilongjiang, China*

[6]*Department of Psychiatry, Qiqihar Medical University, Qiqihar, Heilongjiang, China*

[7]*Key Laboratory of Precise Diagnosis and Neuropsychological Regulation of Mental Disorders, Heilongjiang ， China*

[8]*Department of Clinical Medicine, Harbin Medical University, Heilongjiang 150086, China*

[9]*Department of Basic Medicine, Qiqihar Medical University, Qiqihar, Heilongjiang 161006, China*

[10]*Research Department of Qiqihar Medical University, Qiqihar, Heilongjiang, China*

ABSTRACT: β-ecdysterone, a functional component derived from medicine and food homologous herb *Achyranthes bidentata*, has shown potential in cardiovascular protection according to our previous studies. This study aims to further investigate its neuromodulatory mechanism in cardiac hypertrophy. The anti-hypertrophic effects of β-ecdysterone were validated both *in vivo* and *in vitro*. Transcriptomic analysis of cardiac and medullary tissues revealed the involvement of neuroregulatory pathways, including modulation of sympathetic acitivity. β-ecdysterone significantly reduced norepinephrine (NE) levels and its metabolites, which correlated with hypertrophic markers. Weighted Gene Co-Expression Network Analysis (WGCNA) identified *Dhx37* as a key gene associated with cardiac hypertrophy. In a co-culture model of sympathetic neurons (PC-12) and cardiomyocytes (H9C2), β-ecdysterone suppressed NE secretion and calcium influx in PC-12 cells under Angiotensin II (AngII) stimulation, an effect abolished by *.Dhx37* knockdown in cardiomyocytes. These findings suggest that β-ecdysterone alleviates cardiac hypertrophy by modulating cardiac-sympathetic neuron interaction via the Dhx37 pathway, offering a novel neurocardiac regulatory target for MFH-based therapies.

Keywords: β-ecdysterone; Cardiac hypertrophy; Cardiac-neuro interaction; Multiple omics

1. Introduction

Medicinal and food natural products (MFNPs), widely used in traditional Chinese medicine (TCM), possess both nutritional and therapeutic properties[1, 2]. Notable examples such as ginseng, goji berries, and

†Equal contributors
***Corresponding author**
Dan Xiao, xiaodan@hit.edu.cn.
Yan Lin, yanlinqqhr@aliyun.com..Hui Li, lihui314220@126.com.

Received 20 September 2024
Received in revised from 31 December 2024
Accepted 9 June 2025

astragalus have demonstrated immunomodulatory and antioxidant effects through active components[3-5]. Polysaccharides derived from *Ganoderma lucidum* (Reishi mushroom) enhance immune responses by activating macrophages, natural killer (NK) cells, and dendritic cells (DCs)[6, 7] through receptor-mediated signaling, leading to increased secretion of cytokines such as interleukin-2 (IL3-2) and interferon-gamma (IFN-γ)[8, 9]. *Lycium barbarum* polysaccharides (LBPs) from goji berries exert potent antioxidant effects by scavenging reactive oxygen species (ROS) and reactive nitrogen species (RNS), and by enhancing the activity of antioxidant enzymes such as superoxide dismutase (SOD) and catalase (CAT), thereby reducing oxidative stress-induced cellular damage[10, 11].

Achyranthes bidentata is widely used in TCM, and has demonstrated therapeutica potential in cardiovascular diseases, including ischemic/reperfusion injury[12] and hypertension[13]. Its major bioactive components, including polysaccharides, saponins, and β-ecdysterone, contribute to cardiovascular protection. Among them, *Achyranthes bidentata* polypeptides (ABPP) exert antioxidant and cardioprotection effects[12] by reducing oxidative stress, potentiall via PTEN inhibition and Akt activation. Additionally, β-ecdysterone, a key active compound in *Achyranthes bidentata*, exhibits anabolic effects by promoting protein synthesis, and enhancing muscle mass and strength. It also influences the nervous system[14, 15], with studies reporting cognitive and antidepressant benefits via modulation of neurotransmitter pathways[16]. Although its cardiovascular applications remain underexplored, β-ecdysterone has been shown to reduced hypertrophy and oxidative stress in our previous study by regulationg NRF2 pathway[17].

With the advancement of scientific technology, significant progress has been made in the study of MFNPs. Researchers are exploring the bioactive components and their mechanisms of action using modern biotechnological approaches, such as transcriptomics and metabolomics. For instance, carnobacterium maltaromaticum boosts intestinal vitamin D production to suppress colorectal cancer in female mice by using metabolomic and transcriptomic profiling[18]. The application of lactic acid bacteria fermentation to MFNPs has been shown to significantly increase the content and bioavailability of active components from probiotic properties to the omics insights. This study, therefore, explores the involvement of β-ecdysterone in the neural regulatory mechanisms of myocardial hypertrophy using multiple omics. By integrating metabolomics and multi-organ transcriptomics through weighted gene co-expression network analysis (WGCNA), the study identifies the potential association of the *Dhx37* gene. *In vitro* co-culture experiments with cardiomyocytes and nerve cells further validate the influence of *Dhx37* expression changes in cardiomyocytes on the interaction between these cells, mediating the effects of sympathetic nervous activation on the myocardium.

2. Methods

2.1 Drug-likeness evaluation

Drug-likeness characteristics of the lead compounds were evaluated via absorption, distribution, metabolism, and excretion (ADME) online platform (ADMETlab 3.0, https://admetmesh.scbdd.com/server/evaluation).

2.2 In vivo experimental design

Animal experiments were approved by the Ethic Committees of Qiqihar Medical University. All protocols were complied with the Guide for the Use and Care of Laboratory Animals published by US National Institutes of Health (NIH Publication No. 85-23, revised 1996). Kunming mice (fifty rats, male, 20-25 g) were purchased from the Animal Center of Qiqihar Medical University (Qiqihar, China). All animals were subjected to a 12-h dark/light cycle with a constant humidity of 55% ± 5%.

All mice were fed for 1 week acclimatization, and randomly divided into two parts. Group I: Control group. Animals were administered vehicle only (saline) and normal diet; Group II: Cardiac hypertrophic group treated with ISO only (5 mg/kg, subcutaneously) for 14 consecutive days. Group III: Treatment group, which divided into 1) ISO+0.25 mg/kg β-ecdysterone (ISO+0.25 β-Ecd), 2) ISO+0.5 mg/kg β-ecdysterone (ISO+0.5 β-Ecd), and 3) ISO+1.0 mg/kg β-ecdysterone (ISO+1.0 β-Ecd). Animals were co-treated ISO (i.g.) with β-ecdysterone by gastric gavage route for 14 days. β-ecdysterone (≥ 98% in purity) was purchased from Shanghai yuanye biotech. Co., Ld.

2.3 In vitro experimental design

H9C2 and PC-12 cell lines were cultured with Fresh Dulbecco's modified Eagle's medium (DMEM, Hyclone, Logan, Utah, USA) containing 10% fetal bovine serum (FBS, Gibco, Carlsbad, CA, USA) was added into the culture flask. Cells were transfected with *Dhx37* overexpression plasmid (*Dhx37*-OE) or its blank vector (vector) (RiboBio Co., Ltd., Guangzhou, Guangdong, China). Lipo3000 was used as transfection agent (100 nmol/L) and was dissolved in Opti-MEM serum free medium. After adding the mixture to the cells for 6 h, the medium was replaced by fresh medium. In sympathetic overactivated group, AngII was used and treated for 24 h; In β-ecdysterone treated group (AngII+β-ecd), β-ecdysterone (10 μM, 20 μM, or 40 μM) were treated together with AngII for 24 h. After drug treatment, the cells were used for protein/RNA extraction.

2.4 Real-time PCR

Total RNA was harvested from cells using TRIzol reagent (Invitrogen, Carlsbad, CA, USA) according to the manufacturer's protocols[18]. cDNA synthesis was performed using a High-Capacity cDNA Reverse Transcription Kit (Applied Biosystems, Carlsbad, CA, USA; Cat. no. 4368814) according to the manufacturer's instructions. The levels of *Dhx37* and *Gapdh* mRNA were determined by SYBR Green I incorporation method and ABI 7500 fast Real Time PCR system (Applied Biosystems, USA). Primer pairs were designed according to Primerbank online website (https://pga.mgh.harvard.edu/primerbank/), verified by MFEprimer online website (https://mfeprimer3.igenetech.com/spec), and produced by RiboBio Co., Ltd. (Guangzhou, Guangdong, China). *Gapdh* were used as internal controls. Relative levels were presented as values of $2^{-\Delta\Delta Ct.}$

2.5 Immunofluorescent staining

In brief, cells were fixed, permeabilized, blocked, and then incubated with primary antibodies of Wheat Germ Agglutinin (WGA, Catalog No. W7024, Thermo Fisher Scientific Inc, USA), and examined under an inverted Immunofluorescence microscope (LSM700, Zeiss, Germany).

2.6 Resting-state functional magnetic resonance imaging (rs-fMRI)

A separate cohort of ISO and ISO+β-ecd mice (n = 6 in each group) were used for rs-fMRI analysis. T2-weighed (T2-wt) MRI was performed using a rapid acquisition with relaxation enhancement (RARE) sequence with TR/TE = 4200/36 ms, RARE factor = 8, averaging number = 3. The geometric parameters for the scan were: slice, number = 18, slice thickness = 0.5 mm, matrix = 256 × 256, and FOV = 21 mm^2 × 21 mm^2. Brain volumes in the multi slice T2-wt images were first extracted using an in-house MATLAB program based on the level sets method. The brain images were then registered to the MRI based mouse brain atlas (LONI, UCLA) using affine transformation first, and then nonlinear transformation (DiffeoMap, John Hopkins University, Baltimore, MD). Using the same atlas brain regions were identified and volumes were calculated. A region-by-region comparison was performed between ISO and ISO+β-Ecd groups using one-way ANOVA. Diffusion tensor imaging (DTI) data were acquired using single-shot diffusion-weighted spin-echo echo-planar imaging (TE =43 ms). Acquisition was repeated at TR = 10-15s depending on respiratory rate and one shot per breath. Echo planar imaging (EPI) acquisition parameters included: 14 slices, 200 kHz bandwidth, 96 ×96 in-plane acquisition zero-filled to 256 ×256, and a 0.5-mm slice thickness. Image preprocessing was performed using MATLAB toolboxes and Data Processing Assistant and Resting State fMRI (DPARSF). The preprocessing steps included discarding the first 10 functional volumes, slice timing correction, head motion correction, image normalization, spatial resampling to 3 mm^3 × 3 mm^3 × 3 mm^3, bandpass filtering (0.01–0.08 Hz), and linear detrending.

A sliding-window approach was applied to characterize the dynamic patterns equipped in Dynamic Brain Connectome (DynamicBC) toolbox (V2.2 http://restfmri.net/forum/DynamicBC). Window length is an important parameter in resting-state dynamics computation. A shorter window length may increase the risk of introducing spurious fluctuations in the observed ALFF with window length of 50 TRs (100 s) and a window overlap of 60% (step size by 20 TRs) to compute the ALFF of each mouse. The ALFF maps for each subject were computed within each window, generating a series of ALFF maps. Subsequently, the variance of dALFF maps across time was calculated to measure the temporal variability of intrinsic brain activity.

2.7 Enzyme-Linked Immuno Sorbent Assay (ELISA)

For cardiac tissues and cardiomyocytes *in vitro* culture medium, the Norepinephrine (NE, Catalog No. E-EL-0047, Elabscience Biotechnology Co.,Ltd, Wuhan, China) and parasympathetic neurotransmitter Acetylcholine (Ach, Catalog No. MM-0674M2, Jiangsu Meimian Industrial Co., Ltd, Yancheng, China) were detected by ELISA assays. The protocol was according to the manufacture's instruction.

2.8 Crosstalk Mechanism Mining

2.8.1 Transcriptomics of cardiac and medullary tissues

Using the Illumina sequencing platform, all RNAs of the samples were sequenced, and the high-quality data were compared with the reference genome for further analysis of expression quantification, differential genes, and functional annotation. In this study, transcriptome biochemistry analysis was performed using the Wekemo Bioincloud (Shenzhen, China).

① Sample collection and preparation

RNA was extracted using standard extraction methods, and RNA samples were tested for RNA integrity using the Agilent 2100 bioanalyzer (Agilent Technologies Co. Ltd., United States) for quality control. The mRNA with polyA tails was enriched by Oligo (dT) magnetic beads using the NEBNext® UltraTM RNA Library Prep Kit (Illumina), and the resulting mRNA was subsequently randomly interrupted with divalent cations in the NEB Fragmentation Buffer. The fragmented mRNA was used as a template and random oligonucleotides as primers to synthesize the first strand of cDNA in the M-MuLV reverse transcriptase system, followed by degradation of the RNA strand with RNaseH and synthesis of the second strand of cDNA with dNTPs under the DNA polymerase I system. The purified double-stranded cDNA was end-repaired, A-tailed, and connected to the sequencing junction. The cDNA of 250–300 bp was screened by AMPure XP beads and amplified by PCR, and the PCR products were purified by AMPure XP beads again to obtain the library. After library

construction, initial quantification was performed using a Qubit 2.0 Fluorometer (Thermo Scientific, United States), and the insert size of the library was subsequently checked using an Agilent 2100 bioanalyzer. After the libraries passed the test, Illumina sequencing was performed to generate 150 bp paired end reads.

② Data quality control and differential expression analysis

To ensure the quality and reliability of data analysis, filtration of raw data is necessary. It mainly includes removal of reads with adapter, removal of reads containing N (N indicates that base information cannot be determined), and removal of low-quality reads (reads with Qphred ≤20 bases accounting for more than 50% of the entire read

length). Additionally, clean data were subjected to Q20, Q30, and GC content calculation. All subsequent analyses were based on clean data for high quality analysis. Indexing of the reference genome was constructed using HISAT2v2.0.5 and paired-end clean reads were aligned to the reference genome using HISAT2 v2.0.5. StringTie (1.3.3b) for novel gene prediction. Differential expression analysis between the two compared combinations was performed using the DESeq2 software (1.16.1).

③ Enrichment and pathway analysis

Gene Ontology (GO) enrichment analysis of differentially expressed genes (FDR-adjusted *P*-values < 0.05) was performed using the clusterProfiler (3.4.4) software. Statistical enrichment of differentially expressed genes in KEGG pathways was analyzed using the clusterProfiler (3.4.4) software.

2.8.2 Neurotransmitter metabolomics

① Data process and Normalization

Using unsupervised Principal Component Analysis (PCA), we modeled each group's samples and subsequently displayed score plots based on Hotelling T2 calculations, along with 95% confidence intervals. For sample normalization, the abundance of all features within each sample was divided by the median abundance of that sample. This normalization accounts for library size correction, crucial in addressing substantial variations in total metabolite content observed across samples during the determination process. Such variations often arise from systematic errors introduced during sample collection and analysis. Dividing by the median, mean, or sum is a common approach to correct for this type of systematic error. Content matrix correction involved log transformation of all content values. Methods for differential comparison, such as t-tests and ANOVA, assume that metabolite content follows a normal distribution. Therefore, log transformation is commonly applied to approximate a normal distribution for metabolite content. In feature-wise correction, the abundance of all samples corresponding to a specific feature was subtracted by the mean abundance of that feature and then divided by the standard deviation of the feature's abundance. The aim of feature-wise correction is to standardize the mean and standard deviation (or median, quartiles, scaling) of all metabolites to the same level. Various analyses, including PCA, Partial Least Squares Discriminant Analysis (PLSDA), Orthogonal Partial Least Squares Discriminant Analysis (OPLSDA), and machine learning, benefit from these correction methods.

② Concentration Summary

We calculated the percentage composition of each metabolite within individual samples and visualized the results using a stacked bar chart. This approach provides an intuitive comparison of the differences in metabolite composition structures among different groups, and the displayed the top 20 metabolites by abundance, while the remaining metabolites are grouped under "Others." Barplot was used to present the neurotransmitter content in each sample.

2.9 Weighted gene correlation network analysis

In the context of gene expression profiling, we utilized the Median Absolute Deviation (MAD) for each gene as a starting point. Initially, MAD values were calculated for all genes, and the bottom 50% of genes with the smallest MAD values were excluded. Outliers among genes and samples were further removed using the "good Samples Genes" method from the R software package WGCNA. Subsequently, the WGCNA approach was employed to construct a scale-free co-expression network.

To elaborate, we initially computed Pearson's correlation matrices and applied the average linkage method to all pairwise genes. A weighted adjacency matrix was then created using a power function $A_mn=|C_mn|^{\beta}$ (where C_mn represents Pearson's correlation between Gene_m and Gene_n; A_mn signifies the adjacency between Gene_m and Gene_n). The parameter β served as a soft-thresholding factor, emphasizing strong correlations, and penalizing weak ones. Choosing a power of 6, the adjacency matrix was transformed into a topological overlap matrix (TOM), measuring the network connectivity of a gene by summing its adjacency with all other genes for network generation. The corresponding dissimilarity (1-TOM) was calculated.

To categorize genes with similar expression profiles into modules, average linkage hierarchical clustering was performed based on TOM-derived dissimilarity, with a minimum gene group size of 30 for the genes dendrogram. The sensitivity was set to 3. To delve deeper into the module analysis, dissimilarity of module eigen genes was computed. A cut line for the module dendrogram was chosen, and some modules were merged. Additionally, modules with a dissimilarity less than 0.25 were merged, resulting in a total of 10 co-expression modules. It is noteworthy that the grey module is considered a collection of genes that cannot be assigned to any specific module.

2.10 Statistical analysis

All values were presented as mean ± S.E.M. Statistical comparisons were performed by Student's t-test between two groups or one-way ANOVA for multiple comparisons, and $P < 0.05$ was considered to indicate a significant difference. Data were analyzed using the GraphPad Prism 7.0 software.

3. Results

3.1 β-ecdysterone significantly affects cardiac hypertrophy and neuroregulation-related signaling pathways induced by sympathetic overactivation

Initially, the effects of β-ecdysterone on cardiac hypertrophy in context of sympathetic overactivation were examined by ISO administration or AngII-treated H9C2 cells. Results showed that β-ecdysterone could inhibit the enlarged area of cardiomyocytes in a concentration-dependent manner, compared with sympathetic overactivation (Figure 1). Cardiac transcriptomic analysis of GO and KEGG enrichment analysis revealed that ISO affects extracellular matrix organization, propanoate metabolism, and carbon metabolism pathways (Figure 2A), while β-ecdysterone administration affects neuroregulation-related signaling pathways such as chemical synaptic transmission, neuropeptide signaling pathway, and neuroactive ligand-receptor interaction (Figure 2B). To further explore the potential mechanisms by which β-ecdysterone regulates cardiac sympathetic activity, transcriptomic analysis of the cardiovascular center medulla was performed. Compared to the control group, the ISO group showed changes in metabolic pathways such as fatty acid metabolic process, carbohydrate binding, and thermogenesis (Figure 2C). After β-ecdysterone administration, changes were observed not only in neuroregulation, such as chemical synaptic transmission, positive regulation of cytosolic calcium ion concentration, neuroactive ligand-receptor interaction) but also in cardiac hypertrophy-related pathways (Figure 2D), validating previous conclusions that β-ecdysterone can affect neuroregulation under cardiac hypertrophy conditions. Pharmacokinetic analysis of β-ecdysterone shows disability for crossing the blood-brain barrier (Table S1), we hypothesize that β-ecdysterone may influence neurotransmitter regulation in peripheral cardiac tissue.

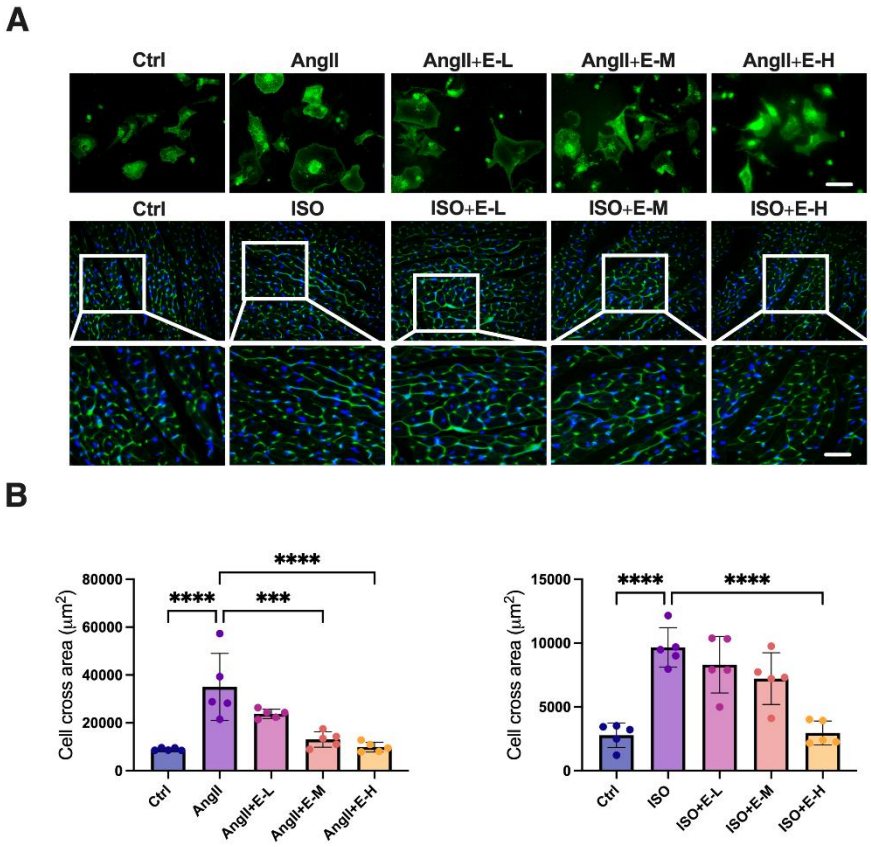
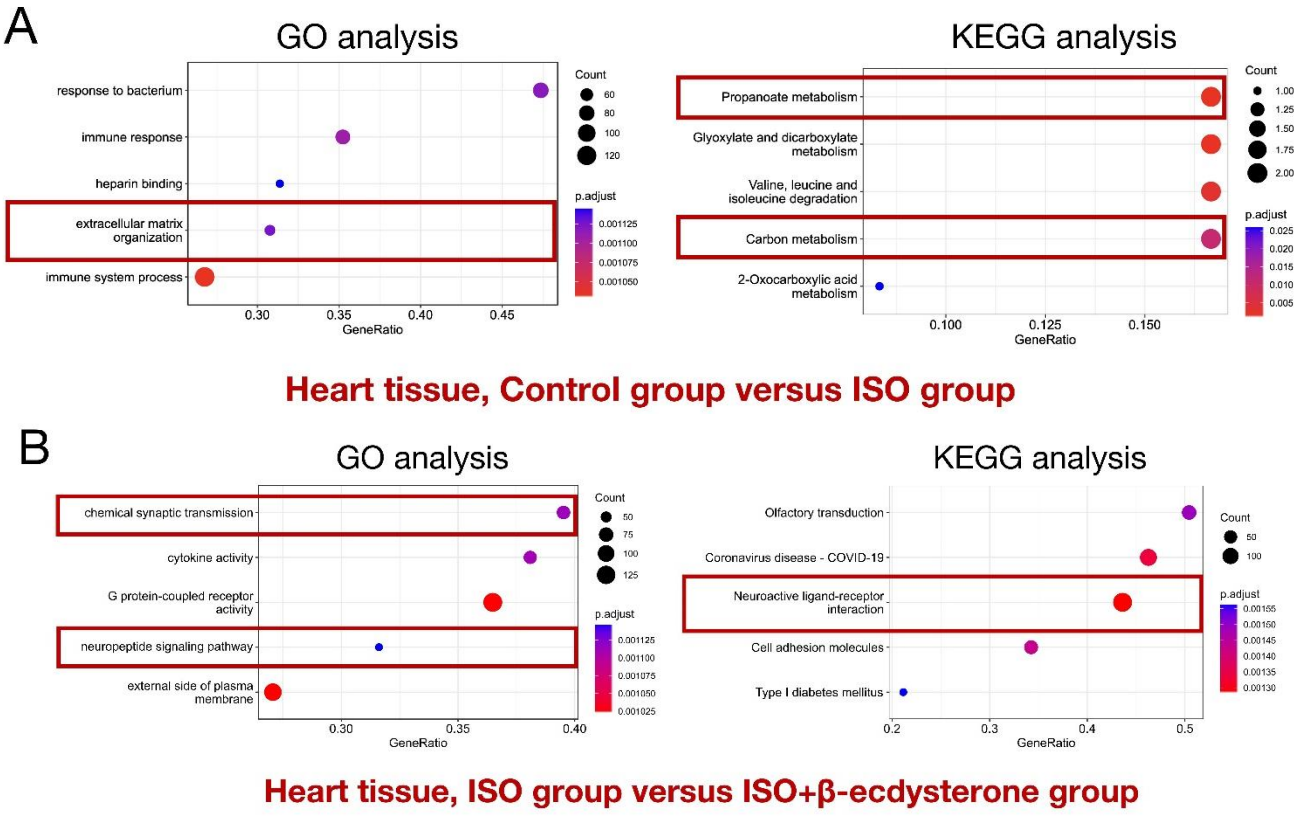


Figure 1. β-Ecdysterone dose-dependently abolished sympathetic nerve activation-induced hypertrophy in cardiomyocytes. (A) The top panel shows representative images of WGA fluorescence staining in H9C2 cells, and the bottom panel shows WGA staining images of cardiac tissue. Scale bar equals 50 μm. E-L represents low-dose β-ecdysterone, E-M represents medium-dose β-ecdysterone, and E-H represents high-dose β-ecdysterone; **(B)** WGA staining statistics: the left panel shows the statistical results of WGA fluorescence staining in H9C2 cells, n=5, ****$P < 0.0001$, and the right panel shows the statistical results of WGA fluorescence staining in cardiac tissue, n=5, ****$P < 0.0001$.



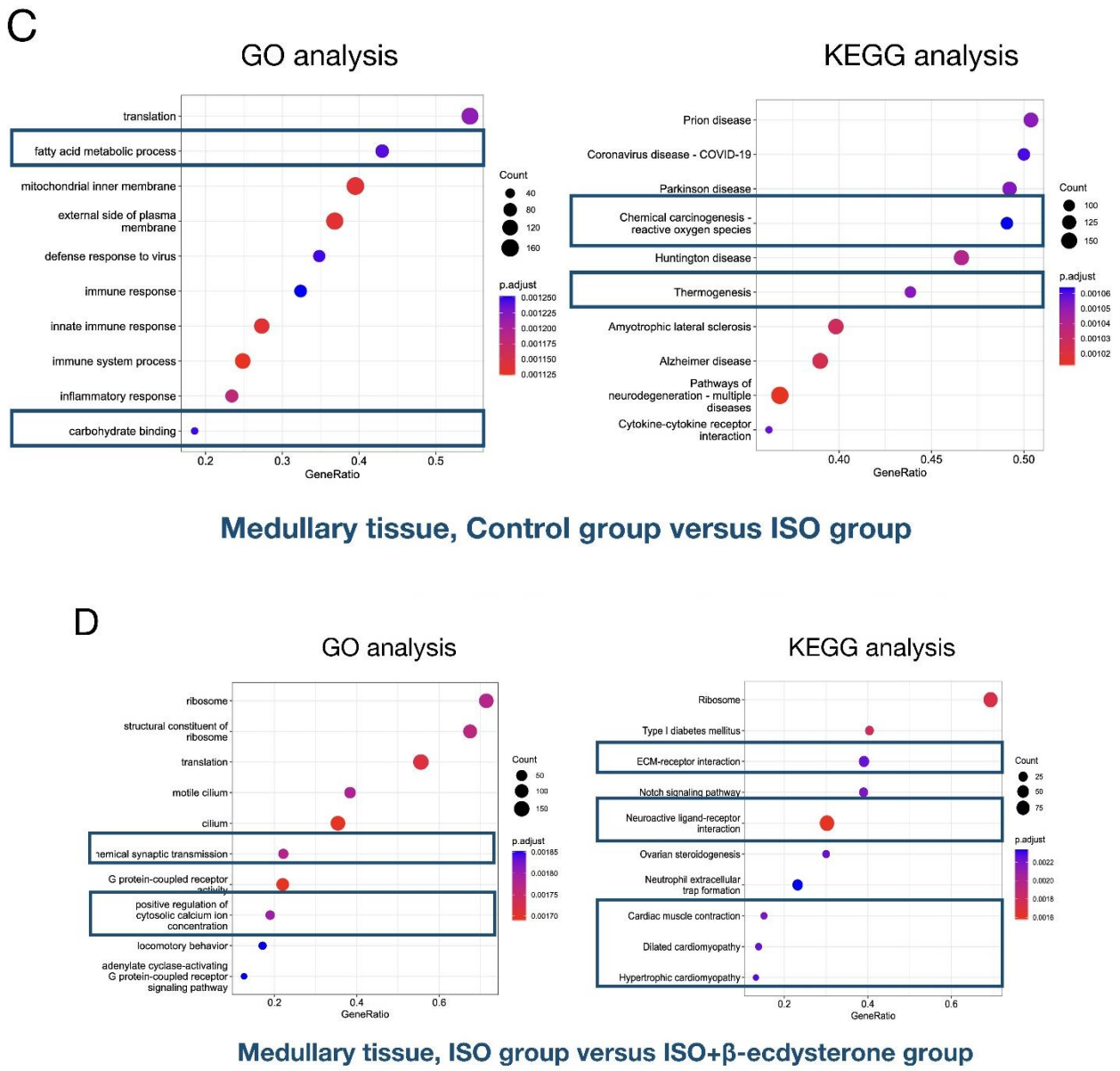


Figure 2. Transcriptomics data of function signaling pathways enrichment analysis heart and medullary tissues. (A, B) In heart tissues, functional enrichment of GO analysis (Top 5) and signaling pathway enrichment of KEGG analysis (Top 5) were presented in comparison of ISO with control group. The red box represents functional/signal pathways associated with cardiac remodeling; **(B)** In heart tissues, functional enrichment of GO analysis (Top 5) and signaling pathway enrichment of KEGG analysis (Top 5) were presented in comparison of ISO+β-ecd with ISO group. The red box represents functional/signal pathways associated with neurotransmitter-related signaling pathways; (C, D) In medullary tissues, functional enrichment of GO analysis (Top 10) and signaling pathway enrichment of KEGG analysis (Top 10) were presented in ISO with control group (C) or ISO+β-ecd with ISO group (D). The blue box represents functional/signal pathways associated with cardiac remodeling and neuroregulation.

3.2 β-ecdysterone inhibits sympathetic neurotransmitter levels in peripheral cardiac tissue

To test this hypothesis, the activity of the sympathetic neurotransmitter norepinephrine (NE) and parasympathetic neurotransmitter acetylcholine in cardiac tissue was first measured. Results indicated that β-ecdysterone significantly reduced norepinephrine levels (Figure S1). Neurotransmitter metabolomics analysis of cardiac tissue, along with correlation analysis with cardiac hypertrophy parameters, revealed β-ecdysterone significantly reduced the sympathetic neurotransmitter NE metabolite 3,4-dihydroxyphenylethyleneglycol (DHPG) compared with sympathetic overactivation group (Figure 3,

Figure S2). Resting-state functional MRI (rs-fMRI) demonstrated that β-ecdysterone administration significantly reduced the activity of the hypothalamic paraventricular nucleus, which is the sympathetic center, compared to the ISO group (Figure S3). In summary, β-ecdysterone treatment inhibits sympathetic activity in cardiac tissue under hypertrophic stimulation, thereby regulating cardiac sympathetic activity.

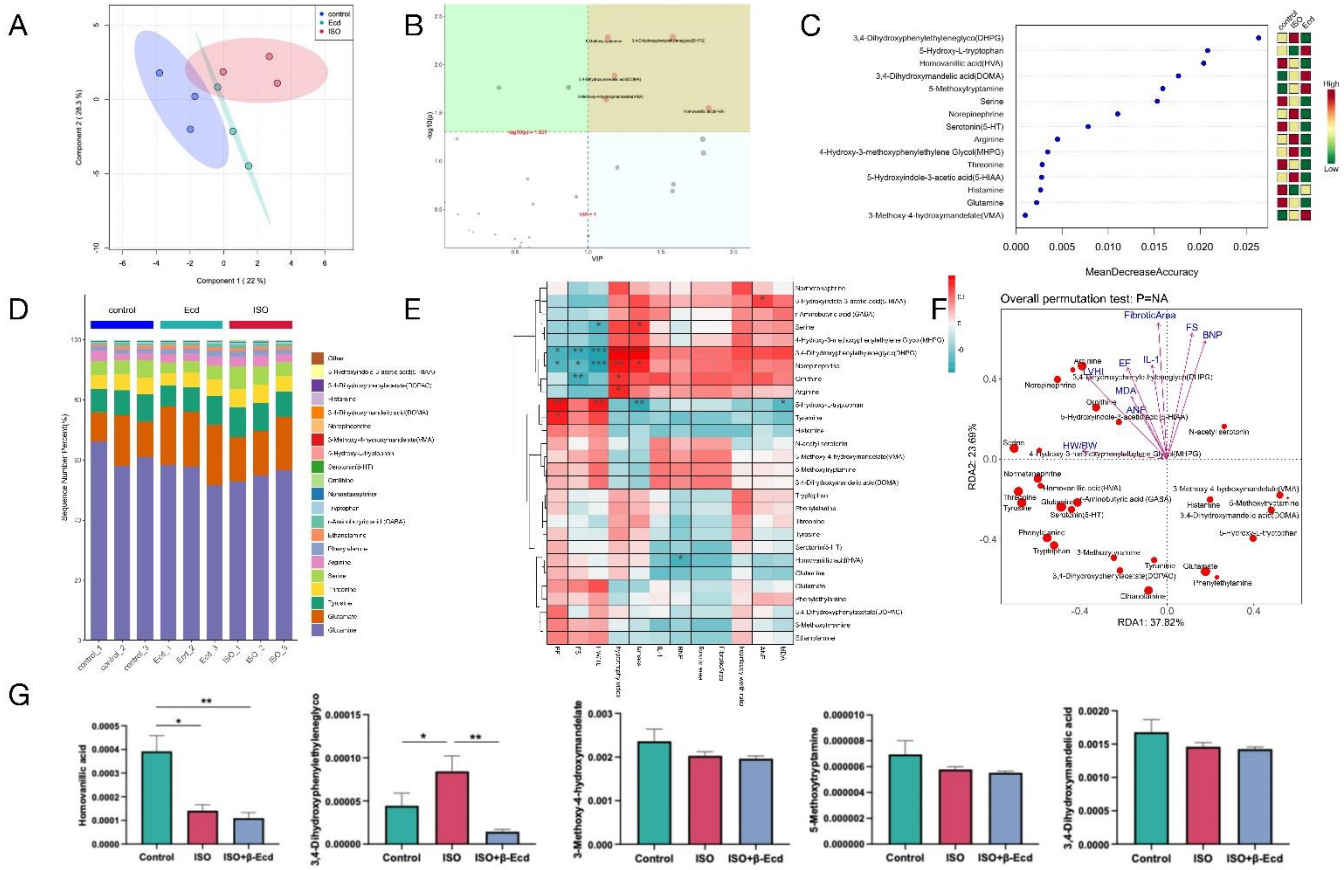
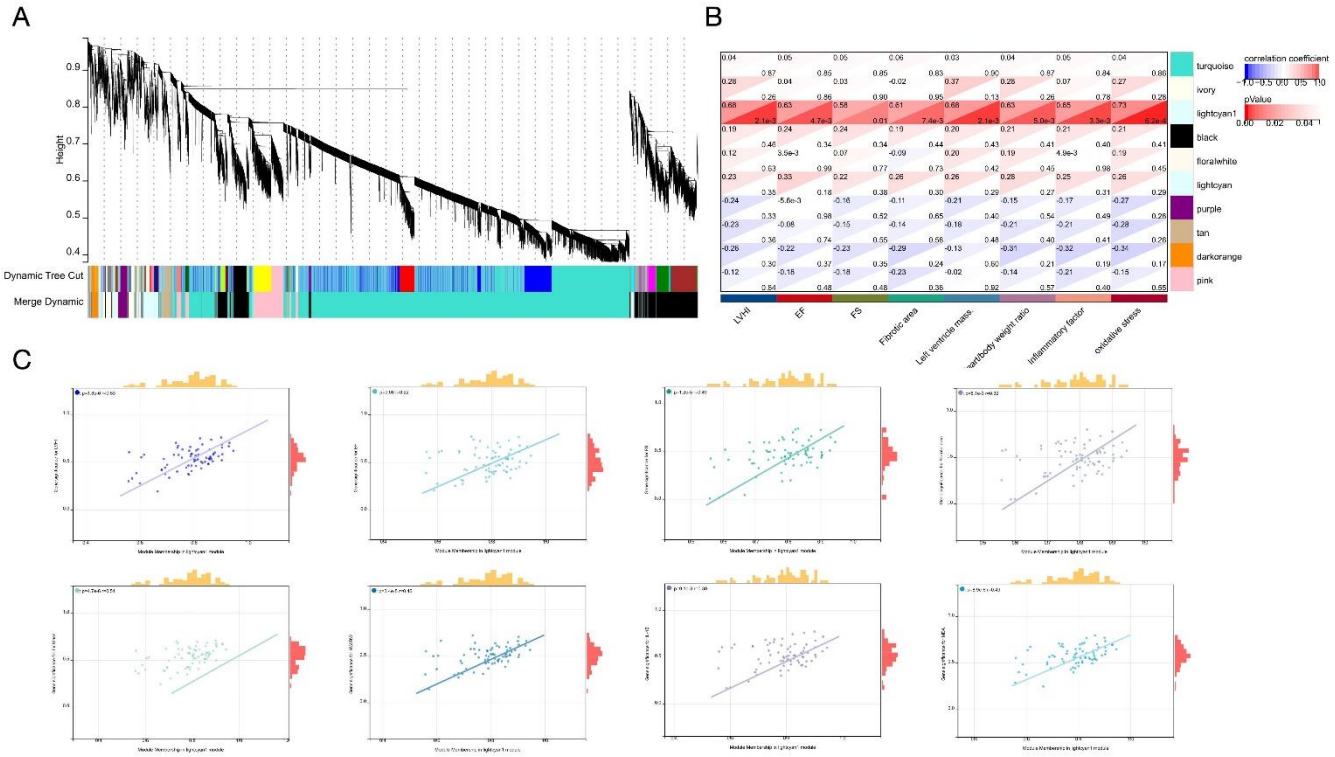


Figure 3. Neurotransmitter metabolomics profiling for other 33 common neurotransmitters in left ventricle of heart tissue. (A) Principal Component Analysis of (PCA) samples, n=3 in each group. (B) Value Importance in Projection (VIP) was performed. The metabolites highlighted in the yellow region are those with a corrected p-value less than 0.05 and a VIP score greater than 1. to identify the metabolites with a VIP score greater than 1 contribute significantly to discriminant analysis, which exhibit substantial differences between groups. (C) Random forest analysis was used with value of "mean decay accuracy" and "mean decay Gini" to measure the importance of a metabolite in distinguishing groups in random forest. The greater the two values, the greater the importance of metabolites in random forests; (D) Percentage content bar chart is used to calculate the top 20 content of metabolites, determining the percentage content of each metabolite within each sample. The results are then visualized using a stacked bar chart, allowing for a straightforward comparison of differences in metabolite composition structure between groups; (E) Correlation analysis between the characterization of cardiac hypertrophy (Cardiac functional index: EF, FS; Cardiac remodeling index: HW/BW & left ventricle hypertrophic index (LVHI); Cardiac hypertrophic index: ANP & BNP; Cardiac fibrosis index: value of fibrotic area; Cardiac inflammation: level of IL-1β; Oxidative stress level: level of MDA and neurotransmitters were performed and then presented as heat map. $*P < 0.05$, $**P < 0.01$, $***P < 0.001$; (F) By employing regression relationship between the characterization of left ventricular remodeling (blue font) and neurotransmitters (red plot) to retain the explainable variations. Dimensionality reduction is applied, and their correlation is indicated using angle measurements; (G) Neurotransmitters of Homovanillic acid (HVA), 3,4-Dihydroxyphenylethyleneglyco (DHPG), 3-Methoxy-4-hydroxymandelate (VMA), 3-Methoxytyramine, 3,4-Dihydroxyphenylacetate (DOPAC) were presented as bar charts. Statistical analysis is performed through inter-group comparisons using the one-way ANOVA method. n=3 in each group, $*P < 0.05$, $**P < 0.01$.

3.3 Dhx37 mediates β-ecdysterone regulation of cardiac-neuro interactions in cardiomyocytes

WGCNA combined with correlation analysis revealed that the lightcyan1 module is significantly correlated with cardiac hypertrophy parameters (Figure 4A-C). Weighted analysis of genes in the lightcyan1 module using Cytoscape identified *Dhx37* as a core regulatory gene in the gene network (Figure 4D). Analysis of *Dhx37* gene expression in cardiac and medulla tissues revealed that ISO upregulates *Dhx37* gene expression in cardiac tissue and cardiomyocytes, while β-ecdysterone downregulates its levels, with no significant changes in the medulla and PC-12 cells (Figure 5A, B). To verify the role of *Dhx37* in cardiac-neuro interactions, we designed *in vitro* experiments: NGF-activated PC-12 cells, which characterized as sympathetic neuron phenotype in previous studies, were co-cultured with H9C2 cardiomyocytes. AngII and β-ecdysterone were added into the cardiomyocyte culture environment. Calcium ion activity and norepinephrine (NE) secretion levels in PC-12 cells were examined, and found that AngII stimulation increased neuronal activity and NE levels, while β-ecdysterone administration inhibited PC-12 activity (Figure 5C). To further verify the role of *Dhx37*, we transfected *Dhx37* over-expression plasmid (*Dhx37*-OE) or its plasmid vehicle (vector) in cardiomyocytes and co-cultured them with NGF-activited PC-12 cells (Figure 6A). *Dhx37*-OE transfection significantly increased *Dhx37* gene expression in H9C2 (Figure 6B) and eliminated the inhibitory effect of β-ecdysterone on PC-12 activity (Figure 6C), as well as NE secretion (Figure 6D). In summary, *Dhx37* in cardiomyocytes mediates β-ecdysterone regulation of cardiac-neuro interactions in context of sympathetic overactivation.



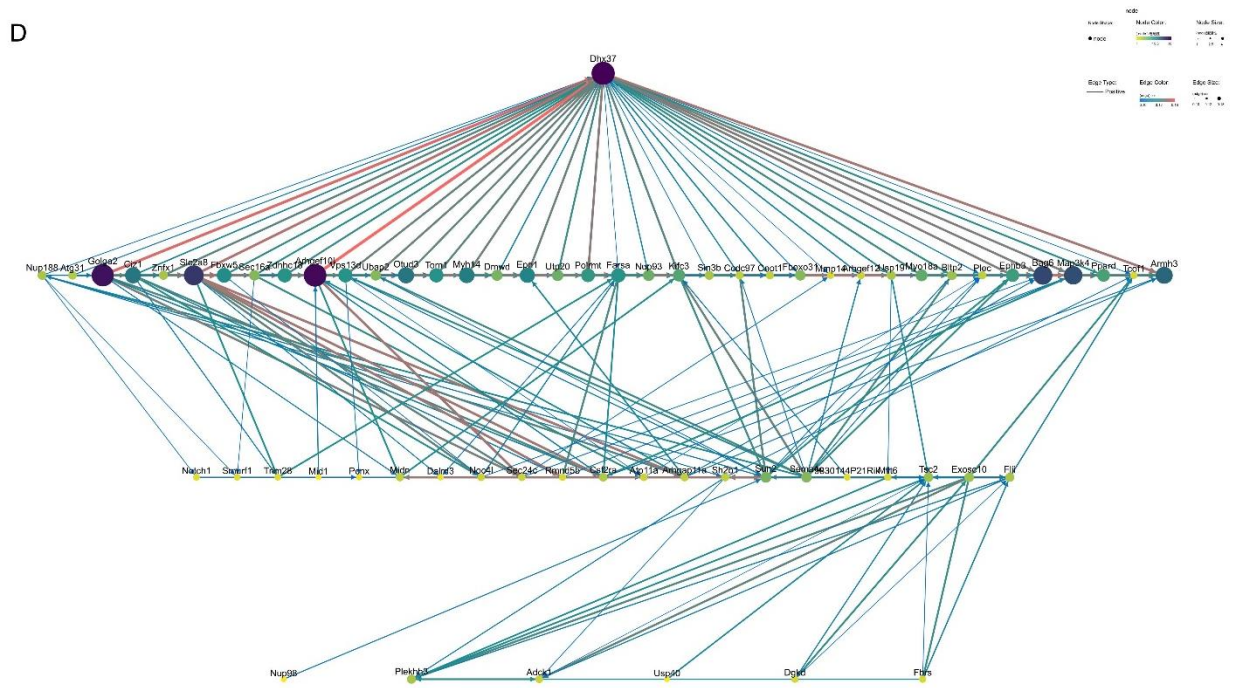


Figure 4. Data mining for the correlation between multi-organ transcriptomics of the heart and medulla with cardiac hypertrophy characteristics. (A) WGCNA analyses were performed among the transcriptomics of heart and medulla tissue among control, ISO, and ISO+β-ecdysterone groups. n=18; (B) Pearson correlation analysis were performed among different module in WGCNA analysis and cardiac remodeling parameters (LVHI, EF, FS, fibrotic area, LV mass, HW/BW, IL-1β and MDA); (C) Linear regression correlation analysis were performed with the module membership in lightcyan module and gene significance with cardiac remodeling parameters of LVHI, EF, FS, fibrotic area, LV mass, HW/BW, IL-1β and MDA; (D) Network of genes in lightcan module were analysis by Cytoscape. The diagram shows the regulatory relationship among the genes, and *Dhx37* is the most important key regulator presented in this network.

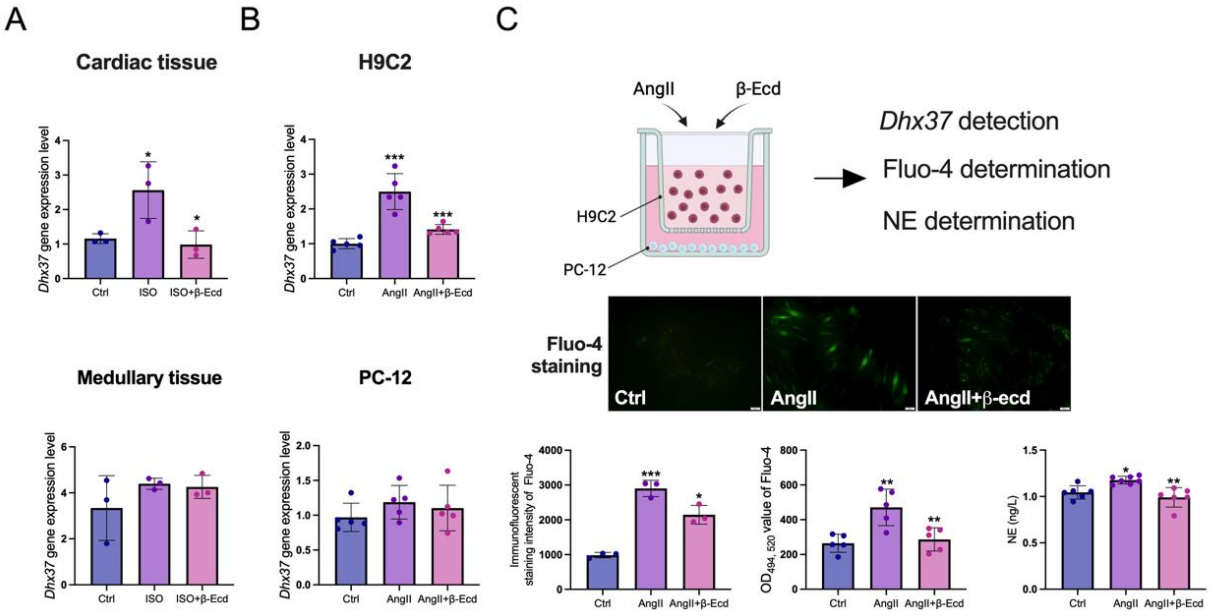


Figure 5. β-ecdysterone-reduced *Dhx37* inhibits the activation of cardiomyocytes by sympathetic nerve cells during sympathetic stimuli. (A) Statistical analysis of Dhx37 gene expression changes in cardiac and medulla tissues based on gene expression levels, n=3, $^{**}P < 0.01$; (B) Statistical analysis of *Dhx37* gene expression changes in H9C2 cardiomyocytes and PC-12 sympathetic nerve cells based on real-time PCR, n=5, $^{***}P < 0.001$; (C) Schematic of co-culture model of H9C2 cardiomyocytes and PC-12 nerve cells (top), with Fluo-4 staining results (middle), and measurements of Fluo-4 fluorescence intensity, Fluo-4 absorbance, and norepinephrine (NE) secretion levels, n=3-5, $^{**}P < 0.01$, $^{***}P < 0.001$.

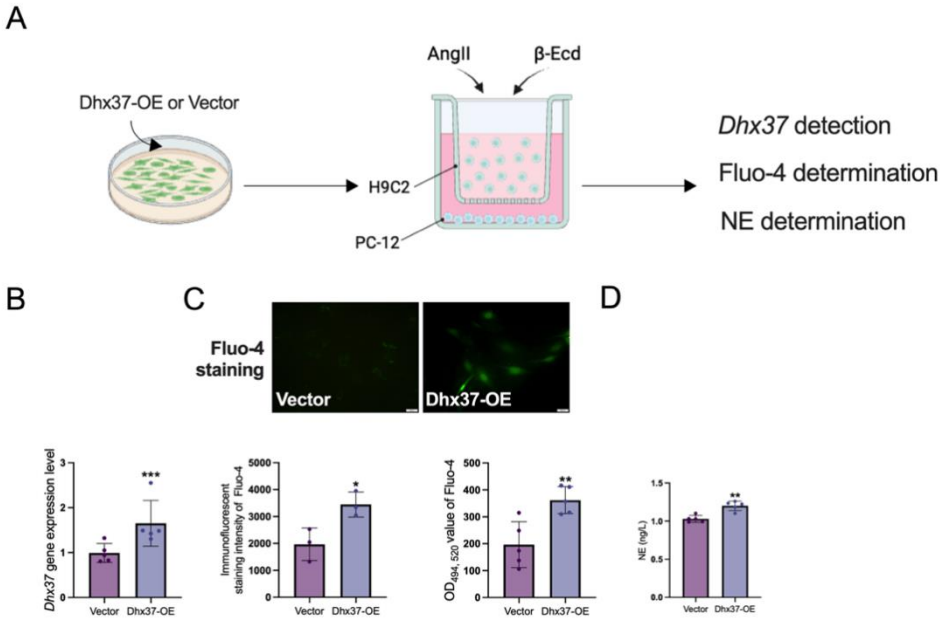


Figure 6. Overexpression of *Dhx37* in cardiomyocytes impedes the inhibitory effect of β-ecdysterone on sympathetic activation induced by sympathetic stimuli. (A) Schematic representation of the co-expression model. Cardiomyocytes were subjected to sympathetic activation stimuli (AngII) and treated with both β-ecdysterone and either *Dhx37* overexpression plasmid or empty vector. Sympathetic activation was then assessed; (B) The transfection efficiency of the *Dhx37* overexpression plasmid in cardiomyocytes was evaluated by real-time PCR, n=5, ***$P < 0.001$; (C) Fluo-4 assay was used to detect calcium channel activity in PC-12 cells. The upper panel shows Fluo-4 staining images, and the lower panel presents the fluorescence quantification, n=3, *$P < 0.05$. Additionally, the fluorescence intensity of Fluo-4 was measured using a microplate reader, n=5, **$P < 0.001$; (D) NE content in the culture medium was measured by ELISA, n=5, **$P < 0.001$.

4. Discussion

Initially, our study has identified three key findings: 1) β-ecdysterone ameliorates cardiac hypertrophy under sympathetic overactiviton. This is significant as it highlights the potential of β-ecdysterone as a therapeutic agent in managing cardiac hypertrophy; 2) β-ecdysterone suppresses the levels of sympathetic neurotransmitters in cardiac tissue, potentially leading to decreased cardiac stress and improved cardiac function. 3) *Dhx37* gene in cardiomyocytes mediates the inhibitory effect of β-ecdysterone on sympathetic nerves, affecting cardiac-neuro interactions. The identification of *Dhx37* as a key mediator in the interaction between β-ecdysterone and the sympathetic nervous system provides a novel insight into the molecular mechanisms underlying the cardioprotective effects of β-ecdysterone, and the role of *Dhx37* on modulating the crosstalk between cardiomyocytes and sympathetic nerves, underscoring its potential as a target for therapeutic intervention.

Sympathetic nervous activation plays a crucial role in the progression of pathological cardiac hypertrophy[19]. The sympathetic nervous system (SNS) becomes overactive in response to various stressors, including hypertension, myocardial infarction, and chronic heart disease, contributing to adverse cardiac hypertrophy[20-22]. Sympathetic activation leads to the release of catecholamines such as NE, which bind to adrenergic receptors on cardiomyocytes[23, 24]. However, prolonged activation results in increased myocardial oxygen demand, ischemia, and further myocardial damage[25, 26]. Research has identified several key genes involved in the regulation of sympathetic nervous activation and its effects on cardiac hypertrophy, for instance, adrenergic receptors (*Adrb1*, *Adrb2*). These receptors mediate the effects of catecholamines on

cardiomyocytes. Genetic variations and expression levels of these receptors influence the degree of sympathetic activation and cardiac response[27, 28]. GRKs, particularly GRK2, regulate the desensitization and downregulation of adrenergic receptors. Overexpression of GRK2 has been associated with heart failure and adverse remodeling[29, 30]. Dysregulation of calcium handling is a hallmark of heart failure. Genes involved in calcium release and reuptake, such as ryanodine receptor 2 (RYR2) and sarcoplasmic/endoplasmic reticulum calcium ATPase2a (SERCA2a), are critical in maintaining calcium homeostasis and cardiac contractility[31, 32]. Thus, understanding the molecular mechanisms and gene targets involved in sympathetic nervous activation and cardiac hypertrophy provides valuable insights for developing targeted therapies. By modulating these pathways, it may be possible to attenuate pathological cardiac hypertrophy and improve outcomes in patients with heart failure.

Notably, the research methods employed in this study, including multiple omics, highlight the increasing prevalence of omics approaches in modern research. With the advent of the omics era, the application of metabolomics and transcriptomics has become increasingly widespread, offering significant insights into biological processes. The combined application of transcriptomics and metabolomics provides a more comprehensive understanding of biological information. For example, integrating gene expression data with metabolite data can more accurately reveal the interactions between gene regulatory networks and metabolic pathways. This multi-omics integrative analysis approach is of great significance in cardiovascular disease research, as cardiovascular diseases often involve complex gene regulation and metabolic abnormalities[33, 34]. A recent study on tobacco roots exposed to hydrogen sulfide used both metabolomics and transcriptomics to reveal key metabolic pathways involved in stress responses. The study found that hydrogen sulfide treatment significantly affected genes and enzymes related to brassinosteroid synthesis and aspartate biosynthesis, promoting root development and potentially reducing pesticide usage[35]. By integrating metabolomics and transcriptomics, researchers can better understand the molecular mechanisms underlying diseases. This approach helps identify biomarkers and therapeutic targets by linking changes in gene expression with alterations in metabolite levels[36]. In pharmacology, combining these two omics techniques accelerates drug discovery and development by identifying drug effects at both the transcript and metabolite levels. These applications highlight the power of integrating metabolomics and transcriptomics to gain a holistic view of biological processes[37-39].

In our study, we also incorporated multi-organ transcriptomics integration, along with complex analyses such as WGCNA and clinical characterization. Through WGCNA analysis, we identified key genes that regulate critical metabolites. For example, by combining transcriptomics with WGCNA, we constructed a metabolic regulation network and uncovered new transcriptional regulatory mechanisms. This approach allowed for correlation analysis between key metabolites like sugars, acids, and volatile esters with gene modules, leading to the identification of modules highly correlated with different metabolites. We further selected structural genes related to sugar metabolism from these highly correlated modules, identified transcription factors based on expression patterns and binding affinity to the structural gene promoters, and

then selected candidate transcription factors for validation based on their correlations[40, 41]. Similarly, by utilizing RNA sequencing data and WGCNA analysis, we identified module genes and miRNAs involved in colorectal cancer, revealing correlations such as that between let-7c-5p and pathological activities like proteoglycans in cancer, focal adhesion, and extracellular matrix (ECM)-receptor interaction[42]. As an advanced method for omics data analysis, this approach is increasingly applied to uncover gene regulation in diseases[43]. Our study leveraged the strengths of this method, applying it to transcriptomics in the heart and cardiovascular central medulla in the context of cardiac hypertrophy, and identified key genes playing significant roles, particularly those influenced by β-ecdysterone.

However, this study has several limitations. The focus of this research was on metabolomics, multi-organ transcriptomics, and correlation characterization. During experimental validation, *in vitro* studies were conducted, but no animal experiments were designed to verify the association between *Dhx37* and heart-neuro regulation at the *in vivo* level. We did not explore in depth the mechanism by which *Dhx37* in cardiomyocytes affects sympathetic nerve activity, such as *Arhgef10l*, which showed the most prominent correlation with *Dhx37* (Figure 4D). Literatures provided the following evidence that high expression of *Arhgef10l* activates the RhoA-ROCK2 pathway[44], where ROCK2 is specifically expressed in cardiomyocytes and associated with angiotensin-induced cardiac hypertrophy[45]. Our current research provides strong evidence for these potentially impactful future studies. Also, further research is warranted to explore the clinical applications of β-ecdysterone in the treatment of cardiac hypertrophy and other related cardiovascular conditions. Additionally, the role of *Dhx37* in heart-sympathetic nerve interactions opens new avenues for targeted therapies aimed at modulating sympathetic activity in cardiac diseases.

Funding

This work was supported by the grants from the National Natural Science Foundation of China (82104173).

Ethical approval

This manuscript meets the criteria for ethical approval.

Conflicts of interest

The authors declared that they have no conflicts of interest regarding this work.

Availability of data and materials

The simulation experiment data used to support the findings of this study are available from the corresponding author upon request.

Acknowledgements

We thank Dr. Yu Jiao and Dr. Xiaoqing Qin for performing rs-fMRI and data analysis.

Reference

1. Sun-waterhouse D. X., Chen X. Y., Liu Z. H., et al. Transformation from traditional medicine-food homology to modern food-medicine homology. Food & Medicine Homology, 2024, 1: 9420014..
2. Zhang T. T., Cai Q. L., Gu Z. Y., Novel ACE-inhibiting peptides from soybean protein hydrolysates by peptidomics combined with in silico analysis and their inhibitory effects on proliferation and migration of AngII-induced VSMCs. Food & Medicine Homology, 2024, 1: 9420023..
3. Cong B. Perspectives in Food & Medicine Homology. Food & Medicine Homology, 2024, 1: 9420018.
4. Liao, L.Y. et al. A preliminary review of studies on adaptogens: comparison of their bioactivity in TCM with that of ginseng-like herbs used worldwide. Chin Med 13, 57 (2018).
5. Zeng, P., Li, J., Chen, Y. & Zhang, L. The structures and biological functions of polysaccharides from traditional Chinese herbs. Prog Mol Biol Transl Sci 163, 423-444 (2019).
6. Gao, X. & Homayoonfal, M. Exploring the anti-cancer potential of Ganoderma lucidum polysaccharides (GLPs) and their versatile role in enhancing drug delivery systems: a multifaceted approach to combat cancer. Cancer Cell Int 23, 324 (2023).
7. Cancemi, G., Caserta, S., Gangemi, S., Pioggia, G. & Allegra, A. Exploring the Therapeutic Potential of Ganoderma lucidum in Cancer. J Clin Med 13 (2024).
8. Mallard, B., Leach, D.N., Wohlmuth, H. & Tiralongo, J. Synergistic immuno-modulatory activity in human macrophages of a medicinal mushroom formulation consisting of Reishi, Shiitake and Maitake. PLoS One 14, e0224740 (2019).
9. Ramberg, J.E., Nelson, E.D. & Sinnott, R.A. Immunomodulatory dietary polysaccharides: a systematic review of the literature. Nutr J 9, 54 (2010).
10. Miranda, M.R. et al. Antitumor Mechanisms of Lycium barbarum Fruit: An Overview of In Vitro and In Vivo Potential. Life (Basel) 14 (2024).
11. Mocan, A. et al. Polyphenols from Lycium barbarum (Goji) Fruit European Cultivars at Different Maturation Steps: Extraction, HPLC-DAD Analyses, and Biological Evaluation. Antioxidants (Basel) 8 (2019).
12. Tie, R. et al. Achyranthes bidentata polypeptides reduces oxidative stress and exerts protective effects against myocardial ischemic/reperfusion injury in rats. Int J Mol Sci 14, 19792-19804 (2013).
13. Mohammed, S.A.D. et al. GJD Modulates Cardiac/Vascular Inflammation and Decreases Blood Pressure in Hypertensive Rats. Mediators Inflamm 2022, 7345116 (2022).
14. Yan, C.P. et al. beta-Ecdysterone Enhanced Bone Regeneration Through the BMP-2/SMAD/RUNX2/Osterix Signaling Pathway. Front Cell Dev Biol 10, 883228 (2022).
15. Wen, F., Yu, J., He, C.J., Zhang, Z.W. & Yang, A.F. beta-ecdysterone protects against apoptosis by promoting autophagy in nucleus pulposus cells and ameliorates disc degeneration. Mol Med Rep 19, 2440-2448 (2019).
16. Phungphong, S., Kijtawornrat, A., Chaiduang, S., Saengsirisuwan, V. & Bupha-Intr, T. 20-Hydroxyecdysone attenuates cardiac remodeling in spontaneously hypertensive rats. Steroids 126, 79-84 (2017).
17. Xiao D, Li R, Lin X, et al. A functional drug discovery in ameliorating cardiac remodeling based on NRF2-regulated oxidative stress. Food Science and Human Wellness, 2025, https://doi.org/10.26599/FSHW.2025.9250500.
18. Echegaray, N. et al. A novel approach to Lactiplantibacillus plantarum: From probiotic properties to the omics insights. Microbiol Res 268, 127289 (2023).
19. Triposkiadis, F. et al. The sympathetic nervous system in heart failure revisited. Heart Fail Rev 29, 355-365 (2024).
20. Hartupee, J. & Mann, D.L. Neurohormonal activation in heart failure with reduced ejection fraction. Nat Rev Cardiol 14, 30-38 (2017).
21. Esler, M. & Kaye, D. Sympathetic nervous system activation in essential hypertension, cardiac failure and psychosomatic heart disease. J Cardiovasc Pharmacol 35, S1-7 (2000).
22. Esler, M. Sympathetic Activation in Essential Hypertension: Understanding the Toxic Trifecta. Heart Lung Circ 27, 271-273 (2018).
23. Waxenbaum, J.A., Reddy, V. & Varacallo, M. Anatomy, Autonomic Nervous System, in StatPearls (Treasure Island (FL); 2024).
24. Elenkov, I.J., Wilder, R.L., Chrousos, G.P. & Vizi, E.S. The sympathetic nerve--an integrative interface between two supersystems: the brain and the immune system. Pharmacol Rev 52, 595-638 (2000).

25. Tibaut, M., Mekis, D. & Petrovic, D. Pathophysiology of Myocardial Infarction and Acute Management Strategies. Cardiovasc Hematol Agents Med Chem 14, 150-159 (2017).
26. Liu, Y. et al. Treatment of Oxidative Stress with Exosomes in Myocardial Ischemia. Int J Mol Sci 22 (2021).
27. Tutgun Onrat, S., Dural, I.E., Yalim, Z. & Onrat, E. Investigating changes in beta-adrenergic gene expression (ADRB1 and ADRB2) in Takotsubo (stress) cardiomyopathy syndrome; a pilot study. Mol Biol Rep 48, 7893-7900 (2021).
28. Guerra, L.A. et al. Genetic polymorphisms in ADRB2 and ADRB1 are associated with differential survival in heart failure patients taking beta-blockers. Pharmacogenomics J 22, 62-68 (2022).
29. de Lucia, C., Eguchi, A. & Koch, W.J. New Insights in Cardiac beta-Adrenergic Signaling During Heart Failure and Aging. Front Pharmacol 9, 904 (2018).
30. Cannavo, A., Liccardo, D. & Koch, W.J. Targeting cardiac beta-adrenergic signaling via GRK2 inhibition for heart failure therapy. Front Physiol 4, 264 (2013).
31. Zhihao, L. et al. SERCA2a: a key protein in the Ca(2+) cycle of the heart failure. Heart Fail Rev 25, 523-535 (2020).
32. Liu, Z. et al. Rg3 promotes the SUMOylation of SERCA2a and corrects cardiac dysfunction in heart failure. Pharmacol Res 172, 105843 (2021).
33. Palou-Marquez, G., Subirana, I., Nonell, L., Fernandez-Sanles, A. & Elosua, R. DNA methylation and gene expression integration in cardiovascular disease. Clin Epigenetics 13, 75 (2021).
34. Sen, P. & Oresic, M. Integrating Omics Data in Genome-Scale Metabolic Modeling: A Methodological Perspective for Precision Medicine. Metabolites 13 (2023).
35. Yang, W. et al. Metabolomics and transcriptomics combined with physiology reveal key metabolic pathway responses in tobacco roots exposed to NaHS. BMC Plant Biol 24, 680 (2024).
36. Maan, K. et al. Metabolomics and transcriptomics based multi-omics integration reveals radiation-induced altered pathway networking and underlying mechanism. NPJ Syst Biol Appl 9, 42 (2023).
37. Blazier, A.S. & Papin, J.A. Integration of expression data in genome-scale metabolic network reconstructions. Front Physiol 3, 299 (2012).
38. Hu, J. et al. Integrating transcriptomics and metabolomics to reveal the protective effect and mechanism of Bushen Kangshuai Granules on the elderly people. Front Pharmacol 15, 1361284 (2024).
39. Connor, S.C., Hansen, M.K., Corner, A., Smith, R.F. & Ryan, T.E. Integration of metabolomics and transcriptomics data to aid biomarker discovery in type 2 diabetes. Mol Biosyst 6, 909-921 (2010).
40. Wang, R. et al. Integrative analyses of metabolome and genome-wide transcriptome reveal the regulatory network governing flavor formation in kiwifruit (Actinidia chinensis). New Phytol 233, 373-389 (2022).
41. Umer, M.J. et al. Identification of key gene networks controlling organic acid and sugar metabolism during watermelon fruit development by integrating metabolic phenotypes and gene expression profiles. Hortic Res 7, 193 (2020).
42. Zhou, X.G. et al. Identifying miRNA and gene modules of colon cancer associated with pathological stage by weighted gene co-expression network analysis. Onco Targets Ther 11, 2815-2830 (2018).
43. Yang, M. et al. Coexpression modules constructed by weighted gene co-expression network analysis indicate ubiquitin-mediated proteolysis as a potential biomarker of uveal melanoma. Exp Ther Med 17, 237-243 (2019).
44. Wang DW, Tang JY, Zhang GQ, Chang XT. ARHGEF10L expression regulates cell proliferation and migration in gastric tumorigenesis. Biosci Biotechnol Biochem. 2020 Jul;84(7):1362-1372.
45. Zhou Q, Wei SS, Wang H, Wang Q, Li W, Li G, Hou JW, Chen XM, Chen J, Xu WP, Li YG, Wang YP. Crucial Role of ROCK2-Mediated Phosphorylation and Upregulation of FHOD3 in the Pathogenesis of Angiotensin II-Induced Cardiac Hypertrophy. Hypertension. 2017 Jun;69(6):1070-1083.